Journal of Theoretical and Applied Physics (JTAP), Vol.16, No. 2, 162211 (1-9), 2022
Received 28 February 2022 ; Accepted 22 April 2022 ; [http://dx.doi.org/10.30495/jtap.162211]

Spin dynamics and surface magnons in antiferromagnetic monoxide lattices along [001] and [011] directions

Mlika Boucherrab, Ouahiba Nafa, Boualem Bourahla*, Farid Chelli

Abstract
A theoretical model to study the localized surface spin states, along two different directions [001] and [011] is presented. The model is mainly used to analyze the antiferromagnetic monoxide network of spins, using the matching method theory. The magnon spectrum is determined by numerical calculations based on the Landauer-Büttiker formalism of the scattering matrix. Our simulation results show the interference effects between magnon states of the monoxide continuum and the localized magnon modes created by the surface region with Fano resonance characteristics.
Additionally, the results are obtained by computing different possibilities of the magnetic parameters, characterizing the antiferromagnetic and the ferromagnetic couplings between spin sites on the monoxide structures. The interactions between the refection and the propagating spin modes describe several types of oscillations. We notice that the magnetic spectra at the surface of monoxide lattices are proportional to the magnetic coupling and the spin intensity of the antiferromagnetic lattices.
Simulations and numerical calculations relating to spin excitations in monoxide lattices make it possible to extract useful information for the elaboration of sensors for specific applications.

Keywords
Spinwaves, Localized spin states, Antiferromagnetic monoxide, Plane surface.

Laboratory of Physics and Quantum Chemistry, Faculty of Science, M. Mammeri University, B.P. 17 RP, 15000 Tizi-Ouzou, Algeria.
***Corresponding author**: boualem.bourahla@ummto.dz

1. Introduction

Many work investigations, from laboratories around the world, are interested in studying all types of oxide structures [1–4]. Their studies are about physical and chemical properties, including structural, electronic and magnetic properties. Oxide structures are very important, due to their unusual properties [5, 6]. We mention, among others, their applications in informatics, electronic, aeronautic and biomedical domains. Indeed, these latter have the advantage to monitor their physical properties by varying external electric and/or magnetic fields.
Nowadays, many efforts have been launched to evaluate the means of storing information technologies and to desire new research for more reliable materials for recording medium purposes. Within this context, special attention is given to better understand the magnetic properties of a specific class of materials that have shown potential application in different domains. We refer mainly to the well know antiferromagnetic monoxides [7].
The knowledge of the magnetic features of the monoxides inevitably passes by the control of the spin fluctuations and spin dynamics [8]. The spin excitations, in these structures are strongly depending on spin coupling, interatomic distances, temperature, surface geometry, magnetic impurities and atomic defects [9, 10]. More precisely, in the industrial domain, the antiferromagnetic monoxide structures can be integrated as elements for information storages [11], or optical telecommunications [12], since their optical and magnetic properties are tremendously important. Additionally, the presence of structural or geometrical inhomogeneities induces large changes and modifications in the magnetic spectra of monoxide structures [13].
For example, it is well established that the magnetic surface properties are very different from those properties, which take place in the case of massive monoxide lattice. In fact, in presence of surface, novel localized magnetic states are created due to the limited range of the spin interactions; at least, in one direction [14]. In general, the presence of the surface leads to the appearance of additional spin branches outside the continuum of the antiferromagnetic perfect monoxide structure. These supplementary branches are labeled localized spin states. They vary greatly with the nature and the geometric shape of the surface. The same magnetic behavior is observed in the case of the magnetic interfaces and/or magnetic imperfections, causing more important localized spin spectra [15, 16], due to the extent of the disturbed zone.
The objective of the current work is to present a theoret-

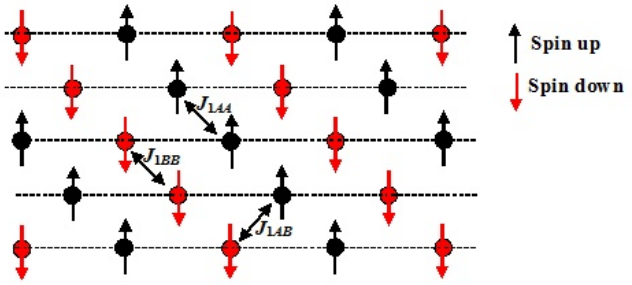

Figure 1. Top view of the spin arrangement at the surface of the MO monoxide structure. The black and red circles indicate up and down metallic spin sites, respectively.

ical study and a numerical calculation, which make it possible to analyze both the spin dynamics and the localized magnon branches generated by the magnetic excitations on the surface layers of modeled MO monoxide antiferromagnetic structure. The localized spin branches present resonant behavior. Particularly, we demonstrate that a plane surface generates resonances and oscillations in the magnonic spectra. The observed resonances come from interactions between localized spinwaves, due the surface domain, and the propagating spinwaves, known as the continuum of the monoxide lattice [17, 18].

In addition, to note the influence of softening and hardening coupling on the magnetic properties, in semi-infinite monoxide lattice, we vary the magnetic exchange and superexchange on the surface layers. The investigation of localized magnonics phenomena, near an antiferromagnetic monoxide plane surface, is conducted by the so-called matching method [19–22], using Heisenberg model [23, 24]. This model allows the calculation of spinwaves localization states and scattering process of spins in a plane surface and at surface boundary.

In section 2, we describe the antiferromagnetic plane surface model and the calculation of the spin fluctuations dynamic in the perfect monoxide waveguide. In section 3, we give the theoretical formalism that allows us to determine the magnon spectra of the spin sites located in the surface layers. In the last section, we present and discuss the numerical spin precession results. The general conclusion of the paper is given.

2. Spin excitation in perfect monoxide structures

Our main interest is to study the spin dynamics at a plane surface of an antiferromagnetic monoxide structure of type MO (M^{+2} is a metallic cation and O^{-2} is an oxygen anion), having a rock-salt crystallization. On the lattice surface, the symmetry of translation is broken in the normal direction (taken z), while the two other directions (x and y) are taken parallel to the horizontal layers that define the plane surface. The surface is considered as a more open system and we can treat them as an inhomogenous magnetic domain, where the semi-infinite structure generates a reduction of the number of adjacent sites. This reduction leads to differences in magnetic coupling between sites belonging to the surface slabs compared to the other sites located in the bulk of the perfect monoxide system.

For each site position, we assign a vector variable, denoted by $\mathbf{S}(l,m,n)$. The indices, $(l,m,n) \equiv p$, are integers that describe the site components in the x, y and z, crystallographic directions, respectively. In addition, we assume that the components S_p^z are perpendicular to the layers of the structure and the surface domain. Figure 1 describes the top view of the spin orientations at the surface of MO monoxide lattice.

The antiferromagnetism of the MO structure is related to a super-exchange phenomenon. We can consider that the MO structure is formed from two interpenetrated sublattices (of the ions M^{2+} and O^{2-}). The first sub-lattice contains spins up and down, respectively. We note a ferromagnetic interaction J_{1AA} and J_{1BB} (between nearest spins of same orientation) and an antiferromagnetic interaction J_{1AB} (between the nearest neighbors of different orientations). In addition, we define the antiferromagnetic interaction J_{2AB} (between the next nearest neighbors).

The antiferromagnetism appears thanks to the presence of O^{2-} anions, diamagnetic atoms located between two magnetic atoms of the cation M^{2+}, whose orbital p is strongly altered by the presence of these two magnetic atoms. The antiferromagnetic symmetry of the metal ion leads to a dilation of the orbital p of oxygen that allows it to reduce its Coulomb energy.

To describe the spin dynamics in antiferromagnetic monoxide, we use the Hamiltonian of the system. The general expression of the latter, for each spin site, is given by

$$H = -\Sigma J_{p\acute{p}} \mathbf{S}_p \mathbf{S}_{\acute{p}} - \Sigma_p D_p (S_p^z)^2 - Bg\mu_B \Sigma_p S_p^z \qquad (1)$$

The first term corresponds to the exchange energy, the second is the anisotropy term with D_l the anisotropy field and the last term corresponds to the Zeeman effect, where μ_B is the Bohr magneton and g is the Landé factor. The latter is neglected in this work, because we have considered the systems far from any external magnetic field.

In the studied monoxide model, we shall consider single particle spinwave excitations, neglecting dipolar interactions and any quantum renormalization procedures for the excitations. In addition, the spin sites are taken ferromagnetically ordered with no loss of generality, with their spins normal to the plane of the surface [25–28].

The parameter $J_{p\acute{p}}$ defines the coupling between the different spin sites; it is said exchange for ferromagnetic type interactions and super-exchange antiferromagnetic couplings.

By considering the spatial periodicity of the spin network, two spins p and $\acute{p}$ which occupy two equivalent sites of the network perform the same magnetic precession motions within one phase. Consequently, their amplitudes verify at each instant t, the following relation

$$\mathbf{u}(\acute{p},\omega) = \mathbf{u}(p,\omega) e^{[i\mathbf{q}.\mathbf{r}(p,\acute{p})]} \qquad (2)$$

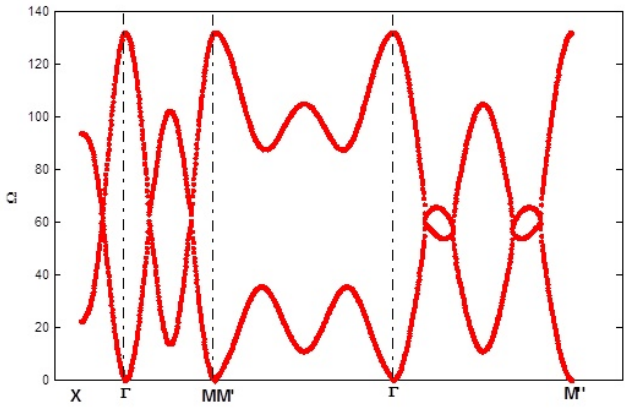

Figure 2. Magnetic dispersion curves in monoxide MO structures, by considering the interactions between nearest and next nearest sites. The path is chosen along the high-symmetry lines.

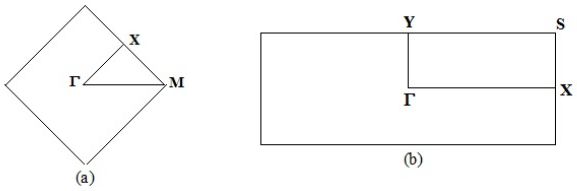

Figure 3. High-symmetry points at the surface of the monoxide MO structure. a) High-symmetry points and Brillouin zone delimitation at (001)-surface of the monoxide. b) High-symmetry points and Brillouin zone delimitation at (011)-surface of the monoxide.

where $\mathbf{q}(q_x, q_y, q_z)$ is a wave vector of the reciprocal lattice and $\mathbf{r}(p, \acute{p})$ the vector joining the site p to the spin site $\acute{p}$.
The equations of the precessional motion of the spins that make up the unit cell in the case of the antiferromagnetic monoxide can be grouped together in the form of a square matrix, denoted D_V [29,30]. We can write them in the form

$$[\Omega I - D_v(\mathbf{q})]|\mathbf{u}\rangle = |0\rangle \tag{3}$$

The matrix $D_v(\mathbf{q})$ constitutes the spin dynamics matrix of the perfect monoxide, with antiferromagnetic interactions, for each $\mathbf{q}(q_x, q_y, q_z)$ data. Moreover, since the x and y axes are plane symmetry directions for the monoxide lattice waveguide, a normalized dimensionless wave vector $\varphi = (\varphi_x, \varphi_y)$ may be introduced, with $\varphi_x = q_x a$ and $\varphi_y = q_y a$; the pair (q_x, q_y, q_z) contains the corresponding reciprocal lattice wavevector components. In the third direction, z-axis, the generic phase factor between neighboring sites is denoted by η, such as $\eta = \exp(j\varphi_z) \equiv \exp(jq_z a)$. The notation I refers to the identity matrix. It has the same size as the dynamic matrix of the perfect monoxide under study, and the vector $|\mathbf{u}\rangle$ contains the components of the eigenvector of the monoxide. Anisotropy is also neglected in this work.
For the system to admit non-trivial solutions, it is imperative to satisfy the following condition

$$\det[\Omega I - D_v(e^{i^*\varphi_x}, e^{i^*\varphi_y}, \eta)] = 0 \tag{4}$$

Equation (4) provides access to dispersion curves. These latter are plotted in Fig. 2.

3. Magnon surface response and localized spin states

In the monoxide surface system, we are interested to highlight and extract the spin sites, which are favorable for the excitation in the three space directions.
In the employed theoretical treatment, the magnetic interactions at the surface and at the boundary of the surface are different from those of the bulk perfect monoxide lattice. These differences are taken into account in our simulations and numerical calculations.
The analysis of the spin excitation in the neighborhood of the surface domain yields a rectangular dynamics matrix, denoted M_d, which contains more unknown variables than equations. Note that the matrix M_d, in the presence of the surface, finds its origin in the writing of the equations of the motion of precession of the spins forming the cell of the defect. These spins are chosen so that the region that contains them includes both spins belonging to the surface region (the three first planes of the surface), as well as those belonging to the connection region presenting an environment of the volume region (the third and the fourth atomic planes from the surface).
The set of these equations of motion constitutes a homogeneous linear system of equations. To this end, we wind up with a matrix M_d, containing 8 equations and 12 unknowns, such as:

$$\lfloor M_d \rfloor |u\rangle = |0\rangle \tag{5}$$

with:$\dim(\lfloor M_d \rfloor) = (8 \times 12)$, $\dim(|u\rangle) = (12 \times 1)$, $\dim(|0\rangle) = (8 \times 1)$.
The notation $|u\rangle$ constitutes a column vector describing the precession amplitudes of all the spins of a unit cell of the perturbed monoxide.
It is important to mention that the elements of M_d are expressed as a function of the exchange and super-exchange parameters that characterize the surface zone and the surface-bulk interface.
In order to establish the matching relations between the precession amplitudes of the spins belonging to the surface domain and the precessional fields of the evanescent modes in the bulk perfect monoxide, we represent the vectors of the sites belonging to the connection region by a linear combination of vectors $|R\rangle$ defining a finite space.
Moreover, the knowledge of the phase factors η, η^{-1}, characterizing the spin evanescent modes due to the presence of the surface, which are determined from the previous study of the perfect monoxide lattice, allows us to make this connection state.

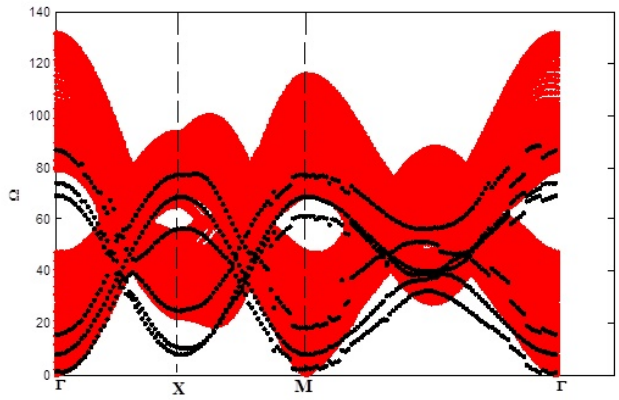

Figure 4. Localized spin branches generated by a plane surface (001) in a monoxide lattices. The continuous red color area describes the bulk energies, whereas the black points represent the localized surface magnon modes. The results are given for the softening spin interactions. The exchange and superexchange spin interaction in the perturbed zone are taken smaller about 20 % than those of the perfect monoxide structures.

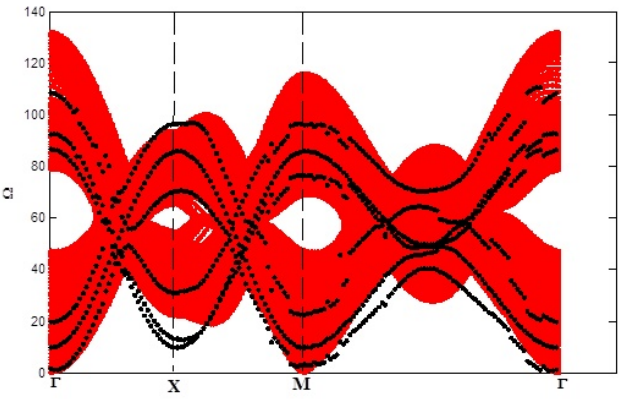

Figure 5. Same results as in Figure 4 for the homogenous spin interactions. In this case, the interactions are taken comparable everywhere, perfect and perturbed zones.

For a spin belonging to the matching region of the surface, its precession amplitudes can be described using the following relation:

$$u_\alpha(n_x,n_y,n_z) = \Sigma_\nu \eta_\nu^{nz} A(\alpha,\nu) R_\nu \tag{6}$$

the parameter α represents the Cartesian directions and $A(\alpha,\nu)$ are the weighted weight coefficients, which are associated with the different evanescent magnon modes ν. They are determined using the cofactors of the volume dynamic matrix D_V defined previously.
The vector $|u\rangle$, describing the precession vectors of all the spins of an elementary cell of the zone considered above, can be divided into two parts:
The first one is denoted by $|irr\rangle$, it consists of the amplitudes of the spin vectors of the irreducible sites forming the region of the surface itself.
The second part denoted by $|rac\rangle$, it is therefore formed by the amplitudes of the spins associated with the matching sites, this for the base $|R\rangle$. Thus, we write:

$$\begin{pmatrix} |irr\rangle \\ |rac\rangle \end{pmatrix} \tag{7}$$

with:$\dim(|irr\rangle) = (6\times 1)$, $\dim(|rac\rangle) = (2\times 1)$.
From there, the matching spin amplitudes can be described using the following expressions:

$$|u\rangle = \begin{pmatrix} |irr\rangle \\ |rac\rangle \end{pmatrix} = \begin{bmatrix} I_d & 0 \\ 0 & R_1 \\ 0 & R_2 \\ 0 & R_3 \end{bmatrix} \begin{pmatrix} |irr\rangle \\ |R\rangle \end{pmatrix} \tag{8}$$

where I_d is an identity matrix of dimensions (6×6); and R_1, R_2 and R_3 are (2×2) matrices given by:

$$R_1 = \begin{bmatrix} \eta_1^2 A(1,1) & \eta_2^2 A(1,2) \\ \eta_1^2 A(2,1) & \eta_2^2 A(2,2) \end{bmatrix}$$

,

$$R_2 = \begin{bmatrix} \eta_1^3 A(1,1) & \eta_2^3 A(1,2) \\ \eta_1^3 A(2,1) & \eta_2^3 A(2,2) \end{bmatrix}$$

, and

$$R_3 = \begin{bmatrix} \eta_1^4 A(1,1) & \eta_2^4 A(1,2) \\ \eta_1^4 A(2,1) & \eta_2^4 A(2,2) \end{bmatrix}$$

, It is useful to remind that the parameters $A(\alpha,\nu)$ represent the weighted coefficients associated with the contribution of the ν^{th} evanescent spin mode along the α-direction. They are determined from the eigenvectors of the perfect MO monoxide lattice. The symbol α designates one of the two space directions (Ox) or (Oy).
The matrix, M_R, is shaped by the dimension (12×8) and is called matching matrix.

$$M_R = \begin{bmatrix} I_d & 0 \\ 0 & R_1 \\ 0 & R_2 \\ 0 & R_3 \end{bmatrix}$$

, The system of Eq.(8) can then be expressed using this matrix as follows:

$$|u\rangle = \begin{pmatrix} |irr\rangle \\ |rac\rangle \end{pmatrix} = \begin{bmatrix} I_d & 0 \\ 0 & R_1 \\ 0 & R_2 \\ 0 & R_3 \end{bmatrix} \begin{pmatrix} |irr\rangle \\ |R\rangle \end{pmatrix} = M_R \begin{pmatrix} |irr\rangle \\ |R\rangle \end{pmatrix} \tag{9}$$

Using this relation, we can rewrite the system of equations (5) above as follows

$$[M_d(8\times 12)][M_R(12\times 8)] \begin{pmatrix} |irr\rangle \\ |R\rangle \end{pmatrix} = |0\rangle \tag{10}$$

Again:

$$[M_s(8\times 8)]\begin{pmatrix}|irr\rangle\\|R\rangle\end{pmatrix}=|0\rangle \tag{11}$$

here, the notation Ms refers to the matrix product between M_d and M_R matrices. The localized surface magnon modes are determined using the following compatibility relation:

$$\det[M_s(8\times 8)]=0 \tag{12}$$

The description of the magnonic localization phenomena on the surface of the monoxide antiferromagnetic lattices requires knowledge of both modes (propagating and evanescent spin modes). These modes are determined by the eigenmodes of the matrix of the perfect monoxide lattice.

4. Numerical applications and discussions

Magnonic properties of the perfect monoxide antiferromagnetic lattice are easily calculated by the diagonalization of the matrix given by equation (2). We obtain two propagating magnon modes. Additionally, the solutions obey to the Bloch condition, defined by the phase factor relation $|Z|=1$.

The spin dispersion branches are presented, in Fig. 2, as a function of the wavevector **q**, when the latter runs in the first Brillouin Zone of the monoxide lattice. The dispersion curve contains two spin modes. These modes correspond to the spins up and down of the cell unit that describe the spin excitation in perfect monoxide antiferromagnetic lattices. We observe that one represents an acoustic mode and the other represents the optical mode. Throughout the text, we numbered the acoustic and optical modes, respectively, by 1 and 2.

The energy of the mode 1 tends to zero, when the wavevector tending to zero. ($\Omega\to 0$, for $q\to 0$). The second mode has a frequency $\Omega\neq 0$, when $q\to 0$.

Along all paths defining the Brillouin zone of the structure, the two magnon modes propagate in the corresponding interval frequency, [$\Omega_{min}=0$, Ω_{max}=133], which represents the energy of the perfect monoxide lattice having the MO structure. The intensity of the exchange and superexchange integrals allow to condition the spin alignment in monoxide structures MO, therefore the nature of the modes and the width of the propagating band are strongly dependent on its parameters. Several authors, in their works [31–33], confirm this claim. In particular, the authors of these studies found that, in most monoxides, the interaction constants between second neighbors are ten (10) times bigger than those of magnetic interactions between the first neighbors [18]. To account for this data, we have numerically determined the magnons dispersion for the following normalized values:

$$\frac{J_{2AB}}{J_{1AA}}=10,\frac{J_{1BB}}{J_{1AA}}=-1$$

The main interest of this work is to examine the spin excitations behavior at the surface layers located around the edge of semi-infinite monoxide cubic structure. More precisely, we focus on the two different crystallographic directions [001] and [011]. In addition, we simulated the effect of varying coupling constants on spin motion, going from softening to hardening of the exchange and super-exchange integrals in the surface domain of the monoxide MO-type structures.

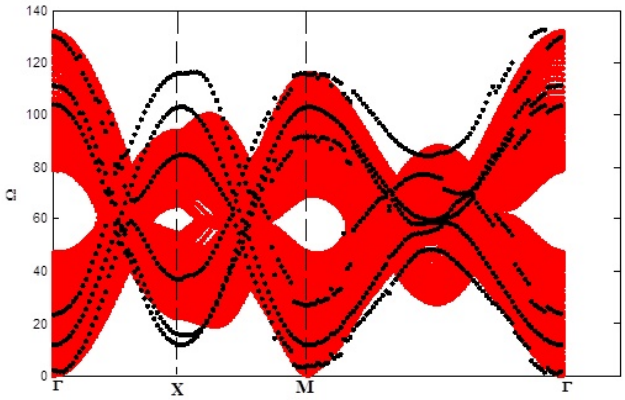

Figure 6. Same results as in Figure 4 for the hardening spin interactions. The situation simulates the case where the magnetic coupling in the perturbed domain are taken higher about 20 % than those of the perfect antiferromagnetic monoxide structures.

The knowledge of the magnonic properties, spinwaves dispersion and spin amplitude precession at the surface can reveal valuable details about monoxide surfaces and magnon properties related to the surface region. Since we are interested in the surface calculation rather than the bulk continuum, we illustrate around each surface direction [001] and [011], the surface magnon branches that occur in specific parts of the Brillouin Zone (BZ).

By using the Eq. (12), we determine numerically the spin energies of the irreducible spin sites located in the surface atomic layers of the modeled monoxide structure with antiferromagnetic interactions.

In this work, the surface localized spin spectra are plotted along all paths defining the BZ, in the two different directions [001] and [011].

In the first direction, [001], the high-symmetry points of the surface are shown in Fig. 3a, while the high-symmetry points, along the second excitation direction [011], are shown in Fig. 3b.

4.1 Surface localized magnon modes along the [001] direction

In the direction [001], the results of localized spin spectra in the antiferromagnetic monoxide model are presented, in Figs. 4, 5 and 6, for the simulated cases of the spin coupling in the surface atomic layers by varying the interface exchange and the superexchange parameters as a function of the normalized energy Ω.

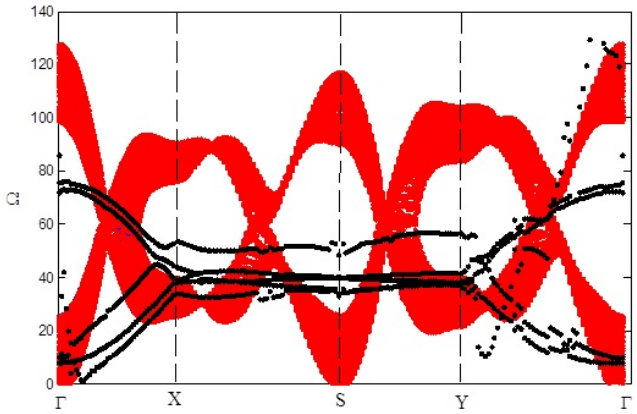

Figure 7. Curves of localized spin states at the limit of the plane surface of the monoxide MO lattice, along the direction [011]. The bulk energies are shown in red, while circular symbols represent localized surface magnon modes. The results are given for the softening spin interactions. The spin-exchange and super-exchange interactions in the disturbed zone are taken to be about 20% smaller than those in the perfect monoxide structure.

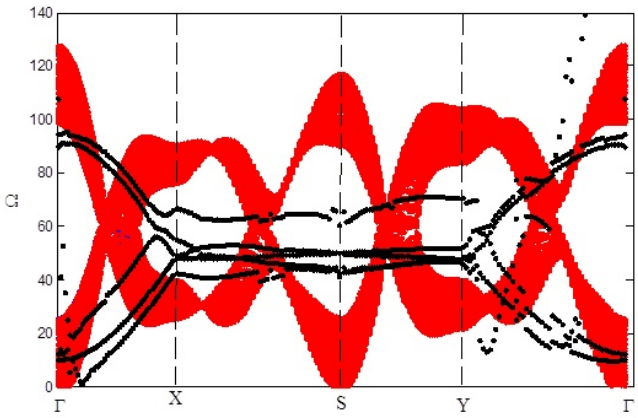

Figure 8. Same results as in figure 7, for the homogeneous spin interactions. In this case, the interactions are taken everywhere comparable, perfect and disturbed zones.

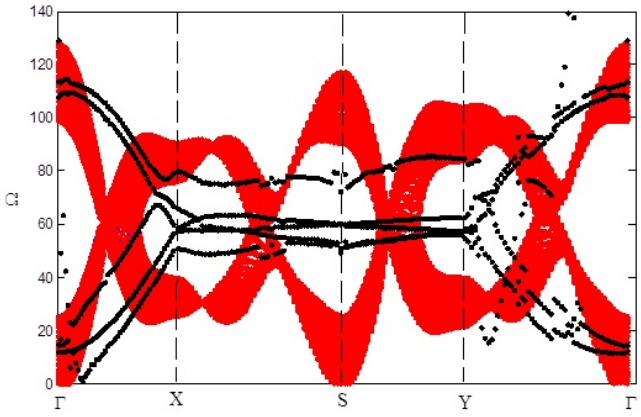

Figure 9. Same results as in figure 7, for the hardening spin interactions. This situation corresponds to the case where the interactions in the disturbed domain are taken to be approximately 20% greater than those of the perfect structure of antiferromagnetic monoxide.

In the first case (Fig. 4), we consider a softening coupling; where the exchange and the superexchange at the surface layers are smaller than the bulk magnetic interactions about 20% [34]. In the second case (Fig. 5), we simulated homogenous environments. The situation describes the case where the magnetic couplings are similar everywhere.

In the last case (given in Fig. 6), we examined the situation where the spin couplings at the plane surface are about 20% higher than the magnetic coupling, describing the hardening situation.

In the three figures 4, 5 and 6, the continuous red color area definite the propagating spin modes for the perfect MO monoxide structure. The bulk states are used as test of control over the numerical calculations.

In all cases, the propagation interval frequency limits of each magnon mode of the continuum are found. They are conforming to the dispersion curve limits.

Notably, in the three various possibilities of the values of the magnetic coupling that we have simulated, the localized spin states represent general and specific characteristics in each case.

We remind that a surface magnon is characterized by its proper frequency, its wavevector and the way; it decays towards the perfect zone. In the localized spin states, we note that the magnon modes become more energetic and its localized branches are displaced to higher energies with increasing the magnetic coupling in the surface domain.

Another general characteristic of the localized spin spectra, for the three studied possibilities, is the displacement of the position frequencies of intersections of the localized spin branches to higher pulsations, but the wavevector position stands stationary with increasing the magnetic exchanges and superexchanges in the surface planes.

We observe a specific plane surface spin precessions in the MO lattice. Principally, we note three types of surface localized spin states:

(i) Rayleigh spinwave modes [35],

(ii) Fuchs-Kliewer spinwave branches [36],

(iii) Microscopic surface spinwave branches [37].

The defined spin modes in (i) and (ii) are characterized by a long penetrating into the MO perfect lattice volume. In addition, the Rayleigh spin modes are often positioned below the acoustic branches of the perfect MO structure, like observed in the softening interactions plotted in Fig. 4. The Fuchs spin modes are positioned in the optical branches, they are clearly observed in Fig. 6. The third type of the mentioned spin modes is located in the gap of the perfect magnonic spectrum. It is observed in Fig. 4. In addition, the comparison between the magnetic spectra makes it possible to note the following remarks:

- Along the high symmetry path ΓX, the energy maximal of the localized branches (given en black color) is observed at the BZ center (Γ), in all cases. Its value is Ω = 87 (for the softening case), Ω = 109 (for the homogenous case) and Ω = 130 (for the hardening situation). We conclude that the localized spin branches generated by the plane surface displace to higher energies with increasing the spin coupling in the surface layers.
- The same behavior is observed in the two others paths XM and MΓ, for three simulated cases. Further, some localized energy branches are degenerate in the high symmetry directions of the system, for three simulated cases. This situation can be explained by the fact that the polarizations of magnon modes of a given spin (up or down orientation) are in a configuration where the precession amplitude on a couplet of sites, in the same layer, or in adjacent layers are symmetric.
- The disappearance of the degeneration informs us about the absence of interference effects in the surface zone. In this case, the polarizations of the spin modes are such that the precession amplitudes on an equivalent couplet of spin sites are antisymmetric.

This situation may be explained by the small wavelengths of the magnon branches in comparison with the lattice parameter. Moreover, we note that in all cases, the localized spin states present several oscillations depending on the coupling parameters at the surface domain. This is a signature of a confinement effect due to the finite extension of the semi-infinite monoxide lattice along the z-axis. Certain maxima picks, observed for $\Omega\varepsilon$ [0, 133], characterize Fano-type resonances; since the spin states on the surface layers are totally localized discrete states and embedded in the incident bulk of the perfect spin waveguide.

- Near the surface zone, the spin dispersion depict spinwaves propagating along the high symmetry directions of the studied surface, which are localized, since their spin amplitude is evanescent in the spin layers perpendicular to the surface.

The localized states provide useful information about the essential characteristics of the surface magnetic coupling and the impact of the bulk-surface interactions on the localized states of the surface spin sites.

In the three simulated cases, the spin-localized branches are the consequence of the reduction of the number of the anion-cation bonds, which decreases the space available for electron delocalization on surfaces, leading to modifications in the band shape, to the appearance of magnon localized surface states in the monoxide spectra.

4.2 Surface localized spin states along the [011] direction

In this direction, the spectra relating to the impact of varying spin interactions, from softening to hardening, on the flat surface of the monoxide MO lattice, are plotted in Figs. (7)-(9). The Fig.7 describes softening interactions, while Fig.8 treats the homogenous case, and the last Fig.9 simulates a hardening situation.

In the three simulated cases, branches in black represent the localized spin states generated by the surface zone of the monoxide lattice, while the red continuous band refers to bulk states of the perfect 3D antiferromagnetic monoxide.

In the three considered environment of spin coupling, it can be seen that the branches of the localized spin states shift towards the high frequencies, along the paths ΓX, XS, SY and YΓ, with the hardening of the exchange and super-exchange integrals at the plane surface.

In fig.7 corresponding to the case of softening of the exchange and super-exchange constants at the plane surface, one might notice the appearance of three localized branches along the paths ΓX and YΓ, barely the bulk band. Furthermore, these localized modes are less energetic. On the other hand, along the paths XS and SY, it can be seen that all the localized surface states are in the volume band. These modes correspond to the Rayleigh surface modes [34] and the microscopic surface modes [37].

In Fig.8 that deals with the case of homogeneity, we notice that the branches of the localized surface states shift towards the high frequencies, along the path of the high symmetry direction, with the emergence of two surface modes the Rayleigh modes and the microscopic modes.

As for the hardening of the exchange and super-exchange integrals at the surface (given in Fig.9), we observe the appearance of two branches above the volume band that are more energetic compared to that of the bulk magnons. In this case, we distinguish the presence of three types of magnon modes located on the surface: Rayleigh modes, Fuchs modes and microscopic surface modes.

The numerical results obtained showed the appearance of new localized states of magnons, which are located near and at the surface. Note that the number and the type of branches depend strongly on the different physical parameters involved in the equations of motion of spin precession. Moreover, in all simulated cases of exchange and super-exchange constants at the monoxide surface, the spectra shows several peaks of oscillations, which are spread over a frequency range [0, 133], that are the corresponding limits to the continuum (perfect antiferromagnetic monoxide lattice). We notice, also, that the peaks have heights and widths that strongly depend on the spin interaction parameters.

We see that certain peaks appear at specific energies. Some of them are associated with different states of localized magnons that are generated near the considered surface, while others correspond to resonance peaks, which are due to Fano-type interactions. These latter are signatures of interference couplings between propagating modes and discrete modes created by the presence of the surface.

At the end, from the obtained results, we conclude that the localized spin states generated by the presence of the surface are strongly dependent on the crystallographic direction, whether of excitation or propagation. This is confirmed by the difference between the spectra of the figures of the two directions [001] and [011] that have been examined, in this work. In

addition, this is foreseeable and expected, as long as the transition from one spin plane to another plane is accompanied by a change in coordination.

5. Conclusion

We have presented a model calculation to study the localized spin states and the magnonic behavior at the plane surface of an antiferromagnetic monoxide lattice, along two different directions [001] and [011]. We have thoroughly established a database of the evanescent magnonic field near the surface plane domain. This makes it possible to determine the evanescent magnon modes.

The theoretical formalism presented, in this work, is an approach based on the matching theory. It is entirely independent of the form and the size of the surface of the monoxide MO antiferromagnetic lattice. The studied magnonic model may be translated to deal with spin fluctuations of other complex surface layers, containing imperfections, or implanted nanostructures. This permits, by analogy, to extend our calculation to other varieties of problem, in magnonic domain.

In all simulated cases (from softening to hardening interactions), the obtained magnetic spectra give rise to valuable information about the exchange and superexchange parameters in the layers of the plane surface or a perturbed zone. Moreover, the magnetic properties are proportional to the spin sites interactions and the spin intensity of the lattice. It is expected that these localized spin states would move to higher energies with increasing the spin interactions in the surface layers, along the different paths that constitute the reduced Brillouin zone of the surface, along the two directions [001] and [011]. We report that simulations and spin numerical calculations have become a very powerful tool for determining the magnonic properties and magnetic spectra of monoxide materials and semicondutors.

Acknowledgments The author B.B. acknowledges financial support provided from DGRSDT of the Algerian Republic. PRFU-Project, registered under the code: B00L02UN150120200001.

Conflict of interest statement:
The authors declare that they have no conflict of interest.

References

[1] M. B. Jungfleisch, W. Zhang, and A. Hoffmann. *Physics Letters A*, **382**:865, 2018.

[2] T. Kampfrath, A. Sell, G. Klatt, A. Pashkin, S. Mährlein, T. Dekorsy, M. Wolf, M. Fiebig, A. Leitenstorfer, and R. H. Uber. *Nature Photonics*, **5**:31, 2011.

[3] Y. Zhu, S. Murali, W. Cai, X. Li, J. W. Suk, J. R. Potts, and R. S. Ruoff. *Advanced Materials*, **22**:3906, 2010.

[4] H. Y. Hwang, Y. Iwasa, M. Kawasaki, B. Keimer, N. Nagaosa, and Y. Tokura. *Nature Materials*, **11**:103, 2012.

[5] T. J. Yen, W. J. Padilla, N. Fang, D. C. Vier, D. R. Smith, J. B. Pendry, D. N. Basov, and X. Zhang. *Science*, **303**:1494, 2004.

[6] Y. Moritomo, Y. Tomioka, A. Asamitsu, Y. Tokura, and Y. Matsui. *Physical Review B*, **51**:3297, 1995.

[7] M. Finazzi, L. Duo, and F. Ciccacci. *Surface Science Reports*, **64**:139, 2009.

[8] M. T. Hutchings and E. J. Samuelson. *Physical Review B*, **6**:3447, 1972.

[9] V. S. Stepanyuk, A. L. Klavsyuk, W. Hergert, A. M. Saletsky, P. Bruno, and I. Mertig. *Physical Review Letters*, **70**:195420, 2004.

[10] A. Delin, E. Tosatti, and R. Weht. *Physical Review Letters*, **92**:057201, 2004.

[11] T. Jungwirth, X. Marti, P. Wadley, and J. Wunderlich. *Nature Nanotechnology*, **11**:231, 2016.

[12] A. Pospischil, M. Humer, M. M. Furchi, D. Bachmann, R. Guider, T. Fromherz, and T. Mueller. *Nature Photonics*, **7**:892, 2013.

[13] M. DiDomenico and S. H. Wemple. *Physical Review*, **166**:565, 1968.

[14] B. Bourahla, O. Nafa, and A. Khater. *Journal of Superconductivity and Novel Magnetism*, **28**:1843, 2015.

[15] P. Mavropoulos and I. Galanakis. *Journal of Physics: Condensed Matter*, **19**:315221, 2007.

[16] G. A. Prinz. *J. Magn. Magn. Mater.*, **200**:57, 1999.

[17] G. Fischer, M. Däne, A Ernst, P Bruno, M Lüders, Z. Szotek, W. Temmerman, and W. Hergert. *Physical Review B*, **80**:014408, 2009.

[18] M. El-Batanouny. *Journal of Physics: Condensed Matter*, **14**:6281, 2002.

[19] L. Djebala and B. Bourahla. *Spin*, **11**:2150014, 2021.

[20] M. Abou Ghantous and A. Khater. *European Physical Journal B*, **12**:335, 1999.

[21] B. Bourahla, A. Khater, R. Tigrine, O. Rafil, and M. Abou Ghantous. *Journal of Physics: Condensed Matter*, **19**:266208, 2007.

[22] O. Nafa and B. Bourahla. *Computational Condensed Matter*, **16**:e00301, 2018.

[23] S. S. P. Parkin, R. Bhadra, and K. P Roche. *Physical Review Letters*, **66**:2152, 1991.

[24] M. Nishiyama, S. Maegawa, T. Inami, and Y. Oka. *Physical Review B*, **67**:224435, 2003.

[25] D. Kriegner, H. Reichlova, J. Grenzer, W. Schmidt, E. Ressouche, J. Godinho, T. Wagner, S. Y. Martin, A. B. Shick, V. V. Volobuev, G. Springholz, V. Holý, J. Wunderlich, T. Jungwirth, and K. Výborný. *Physical Review B*, **96**:214418, 2017.

[26] H. Ohldag, A. Scholl, F. Nolting, S. Anders, F. U. Hillebrecht, and J. Stöhr. *Physical Review Letters*, **86**:2878, 2001.

[27] A. Enders, R. Skomski, and J. Honolka. *Journal of Physics: Condensed Matter*, **22**:433001, 2010.

[28] R. E. Camley and M. G. Cottam. *Physical Review B*, **35**:189, 1987.

[29] A. Khater and M. Abou Ghantous. *Surface Science*, **498**:L97, 2002.

[30] F. Chelli, B. Bourahla, and A. Khater. *International Journal of Modern Physics B*, **34**:2050080, 2020.

[31] C. Franchini, V. Bayer, R. Podloucky, J. Paier, and G. Kresse. *Physical Review B*, **72**:045132, 2005.

[32] J. Kunes, V. I. Anisimov, S. L. Skornyakov, A. V. Lukoyanov, and D. Vollhardt. *Physical Review Letters*, **99**:156404, 2007.

[33] H. Zheng and L. K. Wagner. *Physical Review Letters*, **114**:176401, 2015.

[34] C. de Graaf, R. Broer, and W. C. Nieuwpoort. *Chemical Physics Letters*, **271**:372, 1997.

[35] V. L. Zhang, F. S. Ma, H. H. Pan, C. S. Lin, H. S. Lim, S. C. Ng, M. H. Kuok, S. Jain, and A. O. Adeyeye. *Applied Physics Letters*, **100**:163118, 2012.

[36] F. Li and G. A. Sawatzky. *Physical Review Letters*, **120**:237001, 2018.

[37] A. Kreisel, F. Sauli, L. Bartosch, and P. Kopietz. *European Physical Journal B*, **71**:59, 2009.